Journal of Autoimmunity 75 (2016) 68–81

Contents lists available at ScienceDirect

Journal of Autoimmunity

journal homepage: www.elsevier.com/locate/jautimm

Pro-inflammatory cytokines enhance ERAD and ATF6α pathway activity in salivary glands of Sjögren's syndrome patients

María-José Barrera [a], Sergio Aguilera [b], Isabel Castro [a], Juan Cortés [a], Verónica Bahamondes [a], Andrew F.G. Quest [a, c], Claudio Molina [d], Sergio González [d], Marcela Hermoso [e], Ulises Urzúa [a], Cecilia Leyton [a], María-Julieta González [a, *]

[a] Programa de Biología Celular y Molecular, Instituto de Ciencias Biomédicas (ICBM), Facultad de Medicina, Universidad de Chile, Santiago, Chile
[b] Departamento de Reumatología, Clínica INDISA, Santiago, Chile
[c] Center for Molecular Studies of the Cell (CEMC), Advanced Center for Chronic Diseases (ACCDiS), Faculty of Medicine, Universidad de Chile, Santiago, Chile
[d] Escuela Dental, Facultad de Ciencias, Universidad Mayor, Santiago, Chile
[e] Programa de Inmunología, Instituto de Ciencias Biomédicas (ICBM), Facultad de Medicina, Universidad de Chile, Santiago, Chile

ARTICLE INFO

Article history:
Received 18 April 2016
Received in revised form
21 June 2016
Accepted 15 July 2016
Available online 25 July 2016

Keywords:
Sjögren's syndrome
Salivary glands
Endoplasmic reticulum stress
UPR
ERAD
Cytokines

ABSTRACT

Salivary gland (SG) acinar-cells are susceptible to endoplasmic reticulum (ER) stress related to their secretory activity and the complexity of synthesized secretory products. SGs of Sjögren's syndrome patients (SS)-patients show signs of inflammation and altered proteostasis, associated with low IRE1α/XBP-1 pathway activity without avert increases in apoptosis. Acinar-cells may avoid apoptosis by activation of the ATF6α pathway and ER-associated protein degradation (ERAD). The aim of this study was to evaluate the role of pro-inflammatory cytokines in ATF6α pathway/ERAD activation and cell viability in labial salivary glands (LSG) of SS-patients. In biopsies from SS-patients increased ATF6α signaling pathway activity, as evidenced by generation of the ATF6f cleavage fragment, and increased expression of ERAD machinery components, such as EDEM1, p97, SEL1L, gp78, UBE2J1, UBE2G2, HERP and DERLIN1, were observed compared to controls. Alternatively, for pro- (active-caspase-3) and anti-apoptotic (cIAP2) markers no significant difference between the two experimental groups was detected. Increased presence of ATF6f and ERAD molecules correlated significantly with increased expression of pro-inflammatory cytokines. These observations were corroborated *in vitro* in 3D-acini treated with TNF-α and/or IFN-γ, where an increase in the expression and activation of the ATF6α sensor and ERAD machinery components was detected under ER stress conditions, while changes in cell viability and caspase-3 activation were not observed. Cytokine stimulation protected cells from death when co-incubated with an ERAD machinery inhibitor. Alternatively, when cytokines were eliminated from the medium prior to ERAD inhibition, cell death increased, suggesting that the presence of pro-inflammatory cytokines in the medium is essential to maintain cell viability. In conclusion, the ATF6α pathway and the ERAD machinery are active in LSG of SS-patients. Both were also activated by TNF-α and IFN-γ *in vitro* in 3D-acini and aided in preventing apoptosis. IFN-γ levels were elevated in SS-patients and UPR responses triggered *in vitro* by this cytokine closely matched those observed in LSG from SS-patients, suggesting that cytokines may induce ER stress.

1. Introduction

Sjögren's syndrome (SS) is an autoimmune epithelitis that affects predominantly middle-aged women with a 9:1 female to male ratio [1]. The disease is characterized by periductal lymphocytic infiltration of the salivary and lacrimal glands, which results in reduced secretory functions and oral and ocular dryness [2].

Inflammation and autoimmune diseases have been associated with the accumulation of misfolded/unfolded proteins in the ER, a condition defined as "ER stress" [3,4]. To counteract ER stress, eukaryotic cells activate a series of complementary adaptive

* Corresponding author. Programa de Biología Celular y Molecular, Instituto de Ciencias Biomédicas (ICBM), Facultad de Medicina, Universidad de Chile, Independencia 1027, 8380453, Santiago, Chile.
E-mail address: jgonzale@med.uchile.cl (M.-J. González).

http://dx.doi.org/10.1016/j.jaut.2016.07.006
0896-8411/

mechanisms referred to as the unfolded protein response (UPR) via three transmembrane proteins present in the ER membrane: ATF6α, PERK and IRE1α [4]. While potentially highly relevant to salivary gland (SG) function, little is known the role of UPR in SS-patients [5]. SG acinar cells are secretory cells that show a highly developed rough ER (RER) [6]. Under physiological conditions, SG cells are subjected to high protein synthesis demand, which could induce ER stress [7,8]. Various disorders related to a condition of ER stress have been found in SG from SS-patients, such as intracellular accumulation of mucins [9,10], altered posttranslational processing of MUC5B [11], alterations of Ca^{2+} signaling [12], dilated ER cisternae [13] and high levels of pro-inflammatory cytokines [14]. Previous results from our laboratory revealed that IRE1α/XBP-1s signaling is diminished, suggesting that a chronic condition of ER stress exists in SG of SS patients [15]. Despite this condition of chronic ER stress, levels of apoptosis are low in the SG from SS-patients [16,17], suggesting that other UPR pathways are activated to promote survival, such as ER-associated protein degradation (ERAD). Under ER stress conditions, XBP-1s (IRE1α signaling pathway) and ATF6f (ATF6α signaling pathway) transcription factors regulate expression of various common genes involved in ERAD, and ATF6f activation is particularly associated with chronic ER stress conditions [18–20].

ERAD is essential for the maintenance of cellular homeostasis both under physiological and pathological ER stress [21]. This mechanism involves the recognition, retrotranslocation, ubiquitination and degradation of ERAD substrates by the 26S proteasome [22]. Covalent polyubiquitin conjugation involving multiprotein complexes containing E3 ubiquitin ligases is required for substrate translocation and targeting to the proteasome [23]. The following step involves the extraction of proteins from the ER membrane via the AAA^{+} ATPase p97/VCP complex, which is then shuttled to the proteasome in a tightly coupled sequence [23,24]. Synoviocytes of patients with RA overexpressed HRD1 (Synoviolin), an ER-resident E3 ubiquitin ligase that is involved in ERAD, suggesting hyperactivation of this mechanism in such patients [25,26]. Overexpression of HRD1 in transgenic mice leads to advanced arthropathy caused by reduced apoptosis, whereas HRD1 heterozygous mice ($HRD1^{+/-}$) are resistant to the development of collagen-induced arthritis due to enhanced apoptosis of synoviocytes [25]. Indeed, it has been observed that IL-1β and TNF-α induce synovial cell hyperplasia by upregulating HRD1 expression [26]. Preliminary studies using a cDNA microarray of epithelial cells from labial SG (LSG) of SS-patients revealed up-regulation of genes involved in ERAD, including Ro52, an E3 ligase that participates in quality control of IgG1 immunoglobulins through the ERAD system [27], which also is a main target for auto-antibodies in SS and SLE [28]. Furthermore, SS-patients have anti-20S proteasome autoantibodies [29,30] and overexpress immunoproteasome subunits inducible by IFN-γ [31,32]. In this context, the high levels of pro-inflammatory cytokines present in SG of SS-patients may trigger local stress in the ER and play an important role in the induction and perpetuation of ER stress (chronicity). This being the case, UPR in SS-patients would be expected to trigger mechanisms that do not necessarily lead to apoptosis but rather favor survival, such as ERAD hyperactivity, as has been observed in RA patients [33].

Taken together, these observations suggest that salivary acinar cell survival in SS-patients may be, at least in part, attributable to increased ERAD activation via ATF6α. Bearing this in mind, we analyzed here the localization and expression of ATF6α pathway components and molecules that participate in ERAD in LSG of SS-patients. Also, the effect of pro-inflammatory cytokines on both ERAD and cell survival was studied in extracts from LSG of SS patients and using a three-dimensional (3D) *in vitro* model of acini exposed to pro-inflammatory cytokines.

2. Material and methods

2.1. Patients with SS and controls

A total of 24 individuals participated in the present study after signing an informed consent form based on guidelines established by the Ethics Committee of the Faculty of Medicine, University of Chile. Thirteen individuals were diagnosed as patients with primary SS according to the American/European consensus group criteria [34] and eleven subjects (age and gender matched) were controls. All LSG biopsies from SS-patients had a focus score 1 and around 90% remnant parenchyma could be observed in their LSG. Evaluation of the SG by scintigraphy was performed according to Schall et al. [35]. Scintigraphy results of all patients were classified in four groups: (1) normal, (2) mild, (3) moderate, and (4) severe dysfunction. The controls were selected from individuals who did not fulfill the primary SS classification criteria. All control subjects were negative for rheumatoid factor, antinuclear, Ro and La antibodies. In LSG biopsies from controls, only mild, non-specific, chronic sialadenitis was observed (Chisholm and Mason, grade 1). Individuals with glands showing an advanced degree of fibrosis and/or adiposity were excluded. A detailed description of demographic, serological, and histological characteristics of the SS-patients and controls is summarized in Table 1.

2.2. Biopsies

LSG were obtained as previously described [36]. Samples were immediately frozen in liquid nitrogen and stored at −80 °C to extract RNA and proteins or processed for immunohistochemical analysis.

2.3. Cell culture

The human submandibular gland (HSG) cell line was kindly provided by Professor Bruce Baum (NIDCR, NIH, Bethesda, MD, USA). HSG cells were cultured at 37 °C, 5% CO_2, in DMEM: nutrient

Table 1
Demographic and serological characteristics of the patient and control groups.

	Controls	pSS-patients
No. of individuals	11	13
Gender, no. of (female/male)	9/2	11/2
Age, mean (range), years	42 (21–54)	48 (27–62)
Dry eyes, n (%)	3 (27%)	9 (69%)
Xerostomia, n (%)	1 (9%)	10 (77%)
Focus score[a]		
1	0	13
2	0	0
3	0	0
USWSF, mean ± SD ml 15 min^{-1} (range)	2,5 ± 1,9	1,6 ± 1,3
Scintigraphic data score[b]		
1	2	0
2	7	5
3	2	4
4	0	4
Ro antibodies	0/11	11/13
Ro/La antibodies	0/11	6/13
Antinuclear antibodies	0/11	12/13
Rheumatoid factor	0/11	3/13
Cumulative ESSDAI, median; IQR (25–75)	–	3; 2 (2–4)

n, number; %, percentage; USWSF, Unstimulated whole salivary flow; SD, standard deviation; ESSDAI, EULAR SS disease activity index; EULAR, European League against Rheumatism; IQR, interquartile range.

[a] Number of foci per 4 mm^2 of tissue.

[b] 1 = normal salivary gland function, 2 = mild impairment of salivary gland function, 3 = moderate impairment of salivary gland function and 4 = severe impairment of salivary gland function.

mixture F-12 (DMEM/F-12; Life Technologies, CA, USA) supplemented with 5% characterized fetal bovine serum (FBS; Hyclone, UT, USA), 10,000 U/mL penicillin and 10 mg/mL streptomycin (Biological Industries, Israel). Cells were harvested using 0.25% trypsin/EDTA (Biological Industries, Israel) and suspended in culture media containing 5% FBS. Cells (5×10^5 cells/well) were seeded in six-well plates. After 24 h, they were serum deprived for 24 h to induce differentiation into functional cells. Additionally, a three-dimensional (3D) HSG cell culture system was developed based on the methodology initially described for breast cancer cells [37] and modified for HSG cells in our laboratory. HSG cells were cultured in a semisolid matrix rich in basal lamina proteins extracted from Engelbreth-Holm-Swarm murine sarcoma (Cultrex® Basement Membrane Extract (BME), Trevigen Inc., MD, USA) to induce acinus formation. Initially, 3.5–20 μL of 10 mg/mL BME dissolved in DMEM-F12 were added per well and allowed to solidify at 37 °C for 1 h. Then, 13,500 cells/mL resuspended in DMEM-F12 containing 5% FBS and 0.3 mg/mL BME were seeded per well and incubated at 37 °C and 5% CO_2. After four days, the serum was removed and cells were incubated with serum free medium containing 0.6 mg/mL BME. Differentiated acini obtained after 24 h of serum deprivation were then subjected to the different experimental conditions.

2.4. Treatments

Differentiated 3D-acini were incubated with or without 1 and 10 ng/mL recombinant human TNF-α or IFN-γ (lipopolysaccharide (LPS) free, BioLegend, CA, USA) in serum free medium for 0.5, 3, 6 or 24 h. Subsequently, the cells were lysed to isolate RNA and proteins or processed for immunofluorescence studies as described below. In addition, cells were also treated with the ERAD inhibitor Eerayestatin I (EerI, Calbiochem, Darmstadt, Germany). Initially, EerI concentrations and incubation times were standardized in 2D HSG cell cultures using 0.1, 1, 4 and 8 μM concentrations for 1, 4, 10 and 24 h. Then levels of ubiquitinated proteins were determined by Western blotting. 3D-acini were incubated with 1 ng/mL TNF-α or IFN-γ for 12 h and then with 4 or 8 μM EerI, vehicle (DMSO) or a combination of cytokines plus EerI, for 7 h more. Subsequently, cells were processed to extract proteins or determine cell viability as described below.

2.5. Real time-PCR

Relative levels of mRNA were determined by semi-quantitative real time PCR. RNA extraction, yield and purity were evaluated essentially as described [38]. Primer sequences for the genes studied were designed using the AmplifX 1.4 software (Supplementary Table 1). For PCR reactions, the Brilliant II SYBR Green QPCR Master Mix kit and MxPro-MX 3000P termocycler (Agilent Technologies, CA, USA) were employed. Template cDNA was obtained by reverse transcription of 1 μg of total RNA with SuperScript II Reverse Transcriptase (Invitrogen, CA, USA) and template sequences were amplified by qPCR as described [39]. Target gene levels were standardized to h18S, as previously described using the efficiency-calibrated model [40]. The mRNA expression ratios for the genes of interest standardized to h18S are shown in graphs or box plots. Ratios >1.0 indicate upregulation, and ratios <1.0 are indicative of down-regulation.

2.6. Protein extraction and western blotting

LSG samples and 2D HSG cells culture were homogenized using RIPA buffer and the Complete™ Protease Inhibitor Cocktail EDTA-free Mini Tablets (Roche, Mannheim, Germany). To obtain proteins from 3D-acini without contamination by basal lamina proteins, cells were isolated from BME using Cultrex® 3D Culture Cell Harvesting (Trevigen Inc, Gaithersburg, MD, USA), according to the manufacturer's instructions and then the cells were homogenized with RIPA buffer in the presence of protease inhibitors. Proteins were quantified using the Bradford method [41]. Proteins in a range of 20–50 μg were separated according to their molecular weights by SDS-PAGE on 8 or 12% gels under reducing conditions. Separated proteins were transferred to nitrocellulose membranes (Bio-Rad Laboratories, Hercules, CA, USA) for 15 h at 4 °C. Membranes were blocked for 1 h at room temperature (RT) in 5–12% skimmed-milk (protease-free) prepared in TBST buffer (10 mM Tris HCl [pH 7.5], 150 mM NaCl, 0.1% Tween 20). Blots were then separately incubated with anti-human antibodies (Supplementary Table 2) prepared in TBST buffer for 2 h or overnight at RT. After 5 washes in TBST buffer, membranes were incubated with goat anti-mouse, anti-rabbit or anti-rat HRP-conjugated secondary antibodies for 1 h at RT (Jackson InmunoResearch Laboratories, Inc., PA, USA). Target proteins were detected by chemiluminescence (Pierce, IL, USA). Protein bands were quantified by densitometry. Protein levels were normalized to β-actin.

2.7. Glycosylation state of EDEM1

Proteins (20 μg) of LSG were denatured in 0.5% SDS, 40 mM DTT for 10 min at 100 °C and incubated for 1 h at 37 °C with 50 mM sodium phosphate buffer and 1% NP-40, pH 7.5 and 1000 U of PNGase F (New England BioLabs Inc., MA, USA) in a total volume of 20 μL. Control reactions included proteins treated under the same experimental conditions but in the absence of PNGase F. Samples were then mixed with SDS sample buffer and boiled. Glycan removal was detected as a mobility shift using SDS-PAGE in 8% gels followed by Western blotting with anti–EDEM1 antibody (provided by Stefana-Maria Petrescu, Institute of Biochemistry of Romanian Academy, Bucharest, Romania).

2.8. Immunohistochemistry

LSG were fixed in Bouin's solution and embedded in paraffin wax for histological and immunohistochemical studies. Antigen detection was recovered by incubation with a 0.01 M citrate solution (pH 6.0) for 5 min at 92 °C. All tissue sections were treated with 0.18% v/v of H_2O_2 diluted in methanol for 30 min at RT to inactivate endogenous peroxidase activity. After incubation at RT with 0.25% casein in PBS for 1 h, slides were incubated for 20 h at 4 °C with a 1:50 dilution of the mouse anti-TNF-α antibody (Abcam, MA, USA) or a 1:150 dilution of the rabbit anti-IFN-γ antibody (Abcam, MA, USA). Slides were incubated at RT for 75 min with biotinylated secondary antibody and a streptavidin-peroxidase-conjugated complex (Dako, CA, USA). Slides were developed with DAB chromogen (Dako, CA, USA). Images were captured with a Zeiss (Oberkochen, Germany) light microscope Axiostar plus. For semi-quantification of TNF-α and IFN-γ staining intensity, 20 random acini and 20 random ducts from biopsies of 6 controls and 9 SS-patients were photographed. Staining intensity of three random regions of interest from each image was evaluated using the Image J software (NIH, USA).

2.9. Immunofluorescence

To detect PDI and EDEM1, LSG were fixed in 1% p-formaldehyde (PFA), whereas to detect ATF6α were fixed in Bouin's solution. Then LSG were embedded in paraffin wax. Antigens were recovered by incubation with a 0.01 M citrate solution, pH 6.0, for 25 min at 92 °C for sections fixed in PFA or for 5 min for sections fixed in Bouin's solution. 3D-acini cultured in eight-well chamber slides (Lab-Tek™, Nunc, Thermo Scientific, IL, USA) were fixed in 2% PFA (to detect NF-

κB-p65 or EDEM1) and Bouin's solution (to detect ATF6α) for 15 min at RT. Acini were permeabilized with 1% v/v Triton X-100 in PBS for 10 min and washed three times in PBS containing 100 mM glycine. In both cases, acini and LSG were blocked with 0.25% w/v casein in PBS for 1 h at RT. Then acini were incubated with a 1:300 dilution of the mouse anti-PDI antibody (clone 1D3, Enzo Life Sciences, Inc., NY, USA), a 1:150 dilution of the rabbit anti-EDEM1 antibody (Sigma-Aldrich, MO, USA), or a 1:200 dilution of the mouse anti-ATF6α antibody (Novus Biologicals, CO, USA) for 22 h at 4 °C. After washing slides were incubated with a 1:200 dilution of the Alexa Fluor 488 or 546-conjugated secondary antibodies (Molecular probes Invitrogen, CA, USA). Nuclei were stained with Hoechst 33342 for 1 h at RT. Staining was visualized with a confocal Olympus microscope (model FluoView FV10i, PA, USA). High resolution digital images were captured and stored in TIFF format. As a negative control, rabbit Ig or mouse IgG1 fractions were employed (Dako, CA, USA).

2.10. Deconvolution and colocalization analysis

For colocalization analysis the images were deconvolved with Huygens Professional software (Hilversum, Holland) and then the Manders test was applied to determine colocalization using Imaris 7.2.3 software (Bitplane AG, Zürich, Switzerland).

2.11. Quantitative analysis of the fluorescence staining intensity

Sections of LSG from controls (n = 5) and SS-patients (n = 6) were detected by indirect immunofluorescence analysis using antibodies specific for ATF6α and EDEM1. Images obtained were then photographed at 60X using a confocal Olympus microscope (model FluoView FV10i, PA, USA). Pinhole diameter, intensity and sensitivity laser were maintained between LSG sections from controls and SS-patients for each protein analyzed. Fluorescence intensity (arbitrary unit [AU] per area [μm^2]) was determined by quantifying at least ten full images per section with the ImageJ software (http://imagej.nih.gov/ij/). To determine the fluorescence intensity in epithelial cells, the inflammatory cells were selected using the freehand tool and removed from each image (as is shown in images below). Next, these images were again quantified to calculate the fluorescence intensity present in epithelial cells. Then, the fluorescence intensity of inflammatory cells was obtained subtracting the fluorescence intensity of epithelial cells from full image. Finally, the contribution to fluorescence intensity of the inflammatory cells

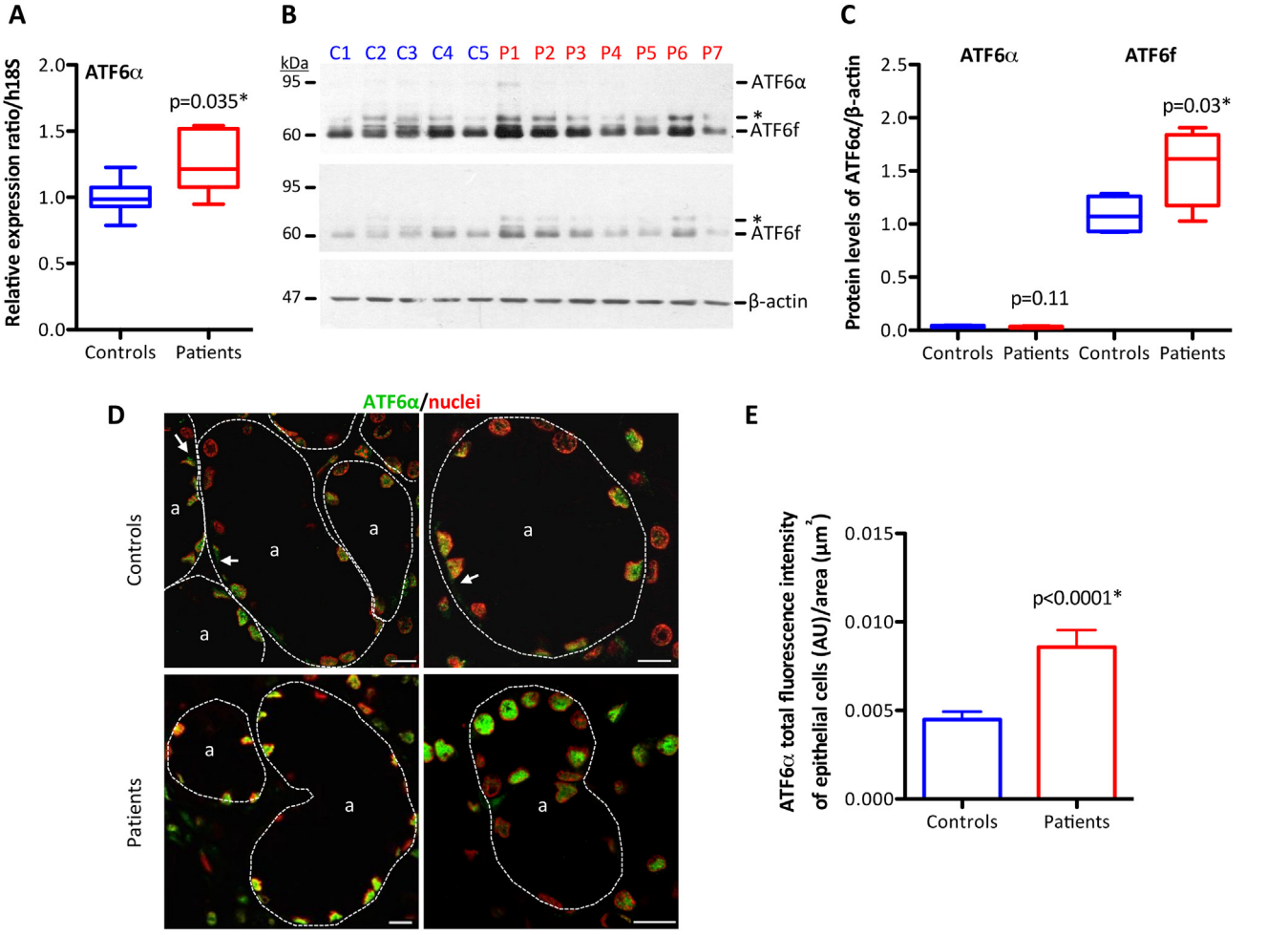

Fig. 1. Increased ATF6α pathway activation in LSG from SS-patients. A, Graph showing transcript levels of ATF6α determined by real-time PCR in samples from 7 controls and 9 SS-patients. **B**, Representative Western blot of ATF6α in LSG extracts from control (C) and SS-patients (P). Here are showed two images, the first overexposed (saturated) in order to view the full-length ATF6α (~95 kDa), because the expression levels of this protein very low and the second with appropriate exposure time to reveal almost exclusively the band of ATF6f (~60 kDa). Also other bands (*) were detected that may be due to intermediate processing of ATF6α. β-actin (~47 kDa) was used as a loading control. **C**, Protein levels of ATF6α and ATF6f relative to β-actin in controls (n = 5) and SS-patients (n = 7) are shown as box plots. **D**, Subcellular localization of ATF6α (green) in LSG from controls and SS-patients. Nuclear staining with Hoechst (red). a: acinus. Bars: 10 μm. **E**, Quantification of total ATF6α fluorescence intensity in epithelial cells of LSG from 5 controls and 6 SS-patients. (*) P values lower than 0.05 were considered significant.

in SS-patients was calculated and compared to the total fluorescence intensity from each image. All these experiments were evaluated by two independent observers.

2.12. Cell viability assay

Cell viability was determined in the presence or absence of EerI or cytokines using the 3-(4,5-dimethyl-thiazol-2yl)-5-(3-carboxymethoxyphenyl)-2-(4-sulfophenyl)-2H-tetrazolium (MTS) reduction assay following the manufacturer's protocol (Promega, WI, USA). Briefly, 3D-acini cultured in flat bottom 96-well plates were serum deprivated for 24 h and then stimulated with cytokines and/or EerI in serum-free medium as described above in a final volume of 100 μL. The plate was incubated for a total time period of 19 h and 20 μL of MTS/phenazine methosulfate solution were then added to each well. The plate was then incubated at 37 °C in a humidified atmosphere containing 5% CO_2 for 4 h. Absorbance at 490 nm was measured and recorded using an ELISA microplate reader (ELX800, BioTek, VT, USA).

2.13. Statistical analysis

All experiments were done at least in triplicate. Normalized data were processed to calculate mean values and standard deviation and are presented in graphs or box plots. The Mann–Whitney *U* test and Pearson's correlations were used for statistical analysis. $P < 0.05$ was considered significant.

3. Results

3.1. ATF6α signaling pathway activation was associated with cytokine-mediated induction in SG from SS-patients

ATF6α is a type II transmembrane glycoprotein that is activated by ER stress and traffics from the ER to the Golgi, where it is cleaved by the proteases S1P and S2P to release a cytosolic fragment (ATF6f) that then translocates to the nucleus to activate transcription of UPR genes [42]. The ATF6α pathway promotes the expression of genes that participate in protein folding and the ERAD system [18–20]. Real time-PCR analysis showed that LSG from SS-patients and controls expressed ATF6α mRNA. However, in SS-patients a significant increase in ATF6α mRNA levels was observed ($p = 0.035$) (Fig. 1A). Activation of the ATF6α transducer was determined by quantifying generation of the ATF6f cleavage fragment. An anti-ATF6α monoclonal antibody was used to detect: i) full length ATF6α with an electrophoretic mobility ~95 kDa (ATF6α) when fully glycosylated; ii) cleavage fragment ATF6f with an electrophoretic mobility ~60 kDa and iii) processed intermediates with electrophoretic mobilities around 70 kDa). ATF6α was difficult to detect in LSG in both groups. Only upon sustained exposure times of membranes to the film was it possible to visualize weakly the ATF6α band in most individuals (Fig. 1B, upper panel), while ATF6f was readily detected in both groups (Fig. 1B). The comparison of ATF6α protein levels showed no statistically significant differences in both groups; however for ATF6f protein levels ($p = 0.03$) a significant increase was observed in SS-patients (Fig. 1C). Lysates of HEK293 cells transfected with human full length ATF6α and HSG transfected with ATF6f transcription factor tagged with influenza

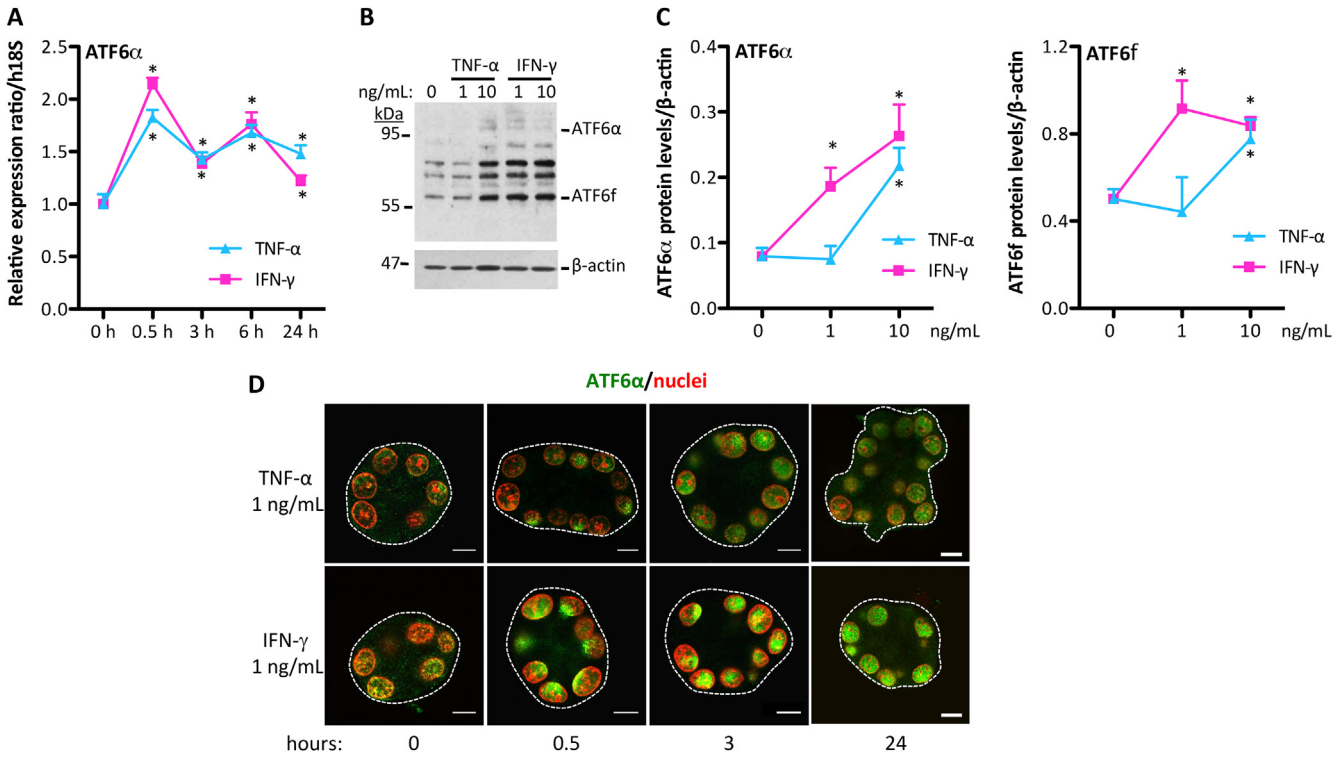

Fig. 2. Activation of the ATF6α pathway in 3D-acini by pro-inflammatory cytokines. **A**, Relative transcript levels of ATF6α in 3D-acini stimulated or not with 1 ng/mL TNF-α or IFN-γ for 0.5, 3, 6 and 24 h. **B**, Representative Western blot of ATF6α in 3D-acini stimulated with 1 and 10 ng/mL TNF-α or IFN-γ for 24 h. **C**, ATF6α and ATF6f protein levels relative to β-actin. (*) P values lower than 0.05 were considered significant. **D**, Subcellular localization of ATF6α (green) in 3D-acini stimulated with 1 ng/mL TNF-α or IFN-γ for 0.5, 3 and 24 h. Nuclear staining with Hoechst (red). a: acinus. Bars: 10 μm. These experiments were replicated at least twice.

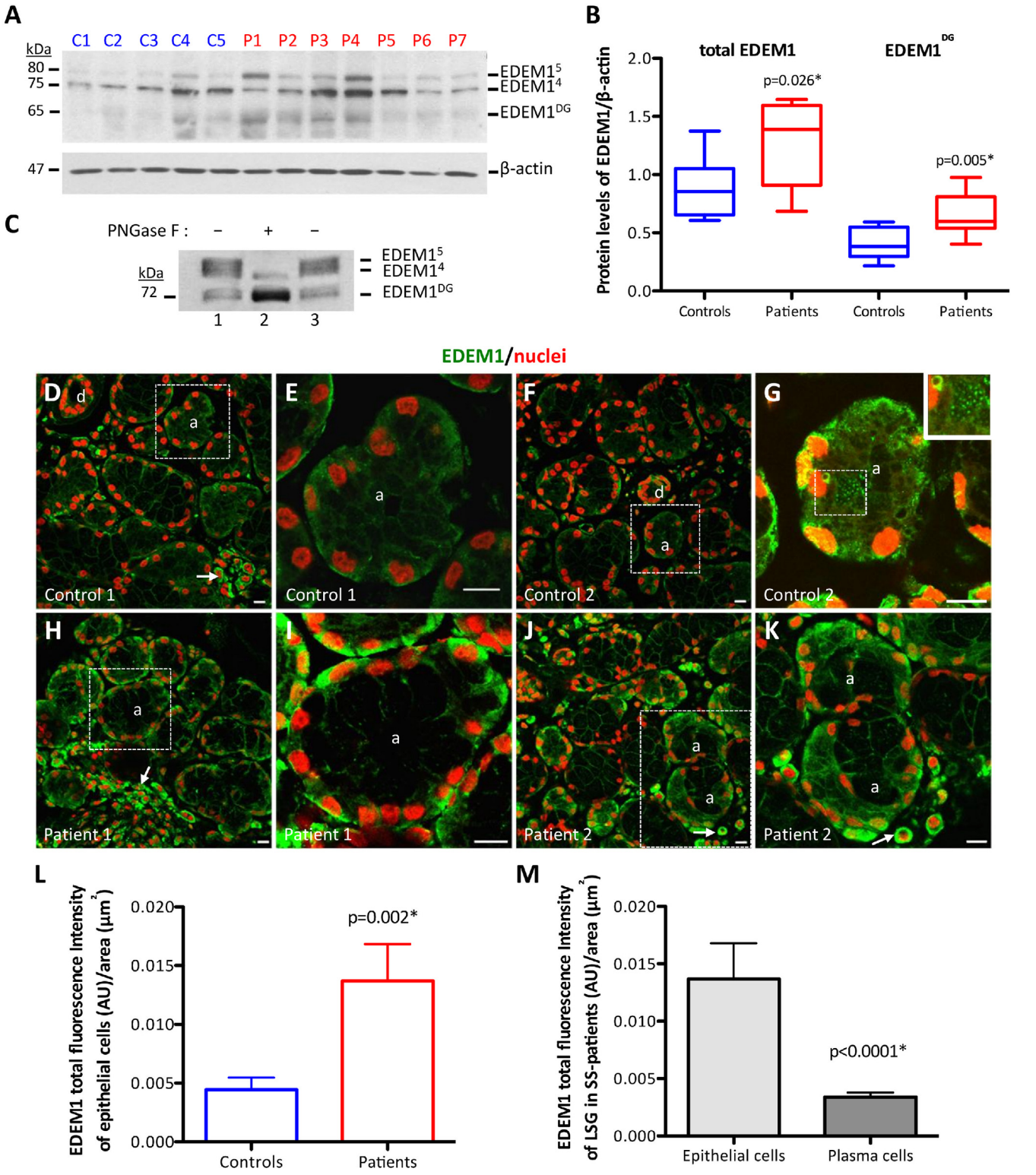

Fig. 3. Expression and localization of EDEM1 in LSG from SS-patients and controls. A, Representative Western blot of EDEM1 in LSG extracts from control (C) and SS-patients (P). Bands of ~80 kDa for 5-fold glycosylated EDEM1 (EDEM1^{5}), ~75 kDa for 4-fold glycosylated EDEM1 (EDEM1^{4}) and ~65 kDa for deglycosylated EDEM1 (EDEM1^{DG}). β-actin (~47 kDa) was used as a loading control. **B**, Protein levels of total EDEM1 (sum of the three bands) and EDEM1^{DG} relative to β-actin in controls (n = 7) and SS-patients (n = 7) are shown as box plots. **C**, N-glycosylation status of EDEM1 was confirmed by deglycosylation using PNGase F in LSG extracts and subsequent detection of EDEM1 by western blotting. Lane 1: protein lysate, Lane 2: PNGase-digested protein lysate, lane 3: protein lysate + enzyme kit without enzyme. **D-K**, Subcellular localization of EDEM1 (green) in LSG sections from controls (D–G) and SS-patients (H–K). The fluorescence intensity of image 3G was saturated to better reveal the punctate structures. Nuclear staining with Hoechst (red). a: acinus, d: ducts. Bars: 10 μm. Arrows: inflammatory cells. **L**, Quantification of EDEM1 fluorescence intensity in epithelial cells of LSG from 5 controls and 6 SS-patients. **M**, Quantification of EDEM1 fluorescence intensity in epithelial and inflammatory cells in LSG from SS-patients. (*) P values lower than 0.05 were considered significant.

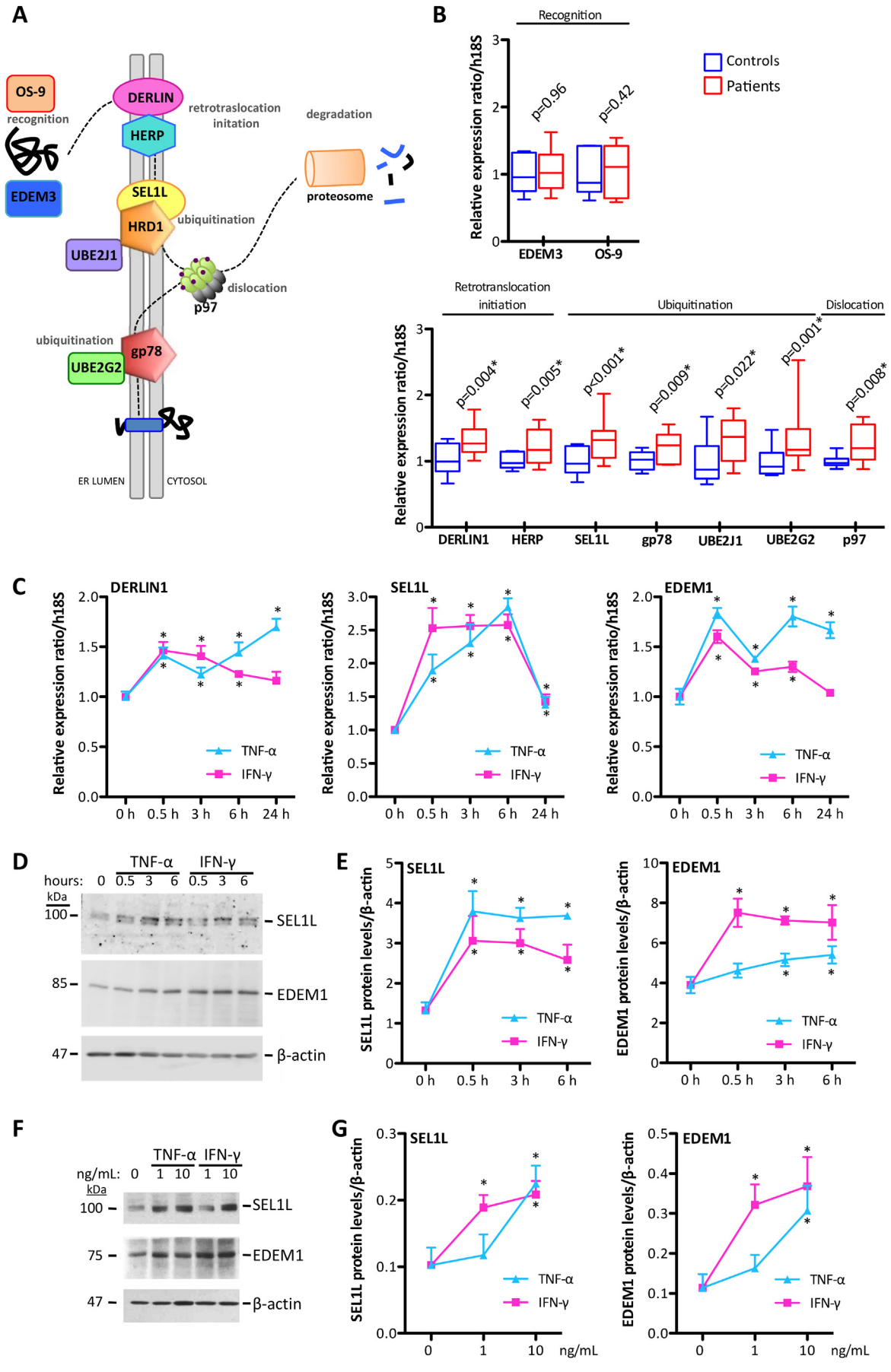
A
OS-9
recognition
EDEM3
DERLIN
HERP
retrotraslocation initation
SEL1L
HRD1
ubiquitination
UBE2J1
degradation
proteosome
dislocation
p97
ubiquitination
gp78
UBE2G2
ER LUMEN
CYTOSOL
B
Recognition
Controls
Patients
Relative expression ratio/h18S
p=0.96
p=0.42
EDEM3
OS-9
Retrotranslocation initiation
Ubiquitination
Dislocation
p=0.004*
p=0.005*
p<0.001*
p=0.009*
p=0.022*
p=0.001*
p=0.008*
DERLIN1
HERP
SEL1L
gp78
UBE2J1
UBE2G2
p97
C
DERLIN1
SEL1L
EDEM1
Relative expression ratio/h18S
TNF-α
IFN-γ
0 h
0.5 h
3 h
6 h
24 h
D
TNF-α
IFN-γ
hours: 0 0.5 3 6 0.5 3 6
kDa
100
85
47
SEL1L
EDEM1
β-actin
E
SEL1L
EDEM1
SEL1L protein levels/β-actin
EDEM1 protein levels/β-actin
TNF-α
IFN-γ
0 h
0.5 h
3 h
6 h
F
TNF-α
IFN-γ
ng/mL: 0 1 10 1 10
kDa
100
75
47
SEL1L
EDEM1
β-actin
G
SEL1L
EDEM1
SEL1L protein levels/β-actin
EDEM1 protein levels/β-actin
TNF-α
IFN-γ
0
1
10
ng/mL

hemagglutinin (HA) were used as positive controls to validate antibody specificity (Supplementary Fig. 1A and B).

Given the importance of the subcellular localization of a protein for appropriate function, ATF6α distribution in LSG sections of SS-patients and control individuals was evaluated. ATF6α mainly localized to the nucleus of acinar cells of both groups (Fig. 1D). Also weak staining for ATF6α was detected mainly for control individuals in the basal perinuclear region, indicative of ER (Fig. 1D, arrows). Quantification of ATF6α fluorescence intensity in different LSG sections (Fig. 1E) revealed a significant, approximately two-fold increase ($p < 0.0001$) in the fluorescence intensity for ATF6α in SS-patients compared to controls. These results are consistent with those obtained by Western blotting, indicating that ATF6α pathway signaling is elevated in SG from SS-patients.

The involvement of pro-inflammatory cytokines in the activation of the ATF6α pathway was probed in a 3D *in vitro* culture model of SG acini, which were generated from cultures of HSG cells grown on a substrate of basal lamina to generate structures with similar morphology and function as SG acini. A significant increase in ATF6α mRNA levels was observed following incubation with 1 ng/mL TNF-α or IFN-γ during 0.5, 3, 6 and 24 h (Fig. 2A). Likewise, protein levels of ATF6α and ATF6f increased significantly with 10 ng/mL TNF-α and with 1 and 10 ng/mL IFN-γ after 24 h (Fig. 2B and C). Also, we evaluated whether pro-inflammatory cytokines induce the nuclear translocation of ATF6α by analyzing 3D cultures stimulated with TNF-α or IFN-γ for either short (0.5 and 3) or prolonged (24 h) periods of time (Fig. 2D). For ATF6α, weak cytoplasmic and nuclear staining was detected in unstimulated acini (Fig. 2D). Following stimulation with TNF-α or IFN-γ for 30 min, ATF6 accumulated in perinuclear (Fig. 2D, TNF-α) or supranuclear (Fig. 2D, IFN-γ) regions and after 3 h elevated nuclear ATF6 staining was observed, suggesting nuclear translocation of ATF6f, which was maintained until 24 h of stimulation (Fig. 2D). IFN-γ appeared more effective than TNF-α in triggering nuclear translocation of ATF6. These results suggest that pro-inflammatory cytokines increase activation of the ATF6α pathway. In addition, TNF-α, IFN-γ and IL-6 expression increased significantly in LSG of SS patients compared to controls (Supplementary Fig. 2), and *in vivo*, acinar cells from LSG of SS-patients also express TNF-α and IFN-γ (Supplementary Fig. 2D and E).

3.2. Increased ERAD activity correlated with inflammation in SG from SS-patients

EDEM1 is a glycoprotein that participates in ERAD of glycoprotein and non-glycoprotein substrates [43]. Following incubation with tunicamycin to induce ER stress, EDEM1 cannot be glycosylated [44]. No significant differences in EDEM1 mRNA levels were found between SS-patients and controls ($p = 0.2$). Polyclonal anti-EDEM1 antibody detected three electrophoretic bands of EDEM1 (Fig. 3A). According to the literature, EDEM1 has five N-glycosylation sites so these bands reflect different degrees of EDEM1 glycosylation [44]. A single site close to the C-terminus is post-translationally glycosylated. Thus, EDEM1 with four or five N-glycosylation modifications ($EDEM1^5$ and $EDEM1^4$), as well as deglycosylated forms ($EDEM1^{DG}$) are frequently observed [44]. $EDEM1^5$ and $EDEM1^4$ are the two bands of lower relative electrophoretic mobility of ~80 and 75 kDa, respectively whereas the ~65 kDa band is due to $EDEM1^{DG}$ (Fig. 3A). Densitometric quantification of total EDEM1 ($EDEM1^{DG}$, $EDEM1^5$ and $EDEM1^4$) and $EDEM1^{DG}$ revealed a significant increase ($p = 0.026$ and $p = 0.005$, respectively) in SS-patients (Fig. 3B). Analysis of samples in gel-shift assays after treatment with the deglycosylating enzyme PNGase F revealed that the band of ~80 KDa was indeed fully glycosylated EDEM1 (see Fig. 3C). In addition, in LSG sections from controls, EDEM1 was detected in the cytoplasm of acinar and ductal cells (Fig. 3D–G) within punctate structures in the cytoplasm of acinar cells (Fig. 3G, the fluorescence intensity of this image was satured to better reveal the punctate structures). In SS-patients, EDEM1 localized mainly to the perinuclear region of acinar cells and was also detected in the cytoplasm of inflammatory cells (Fig. 3H–K). Consistent with the results obtained by Western blotting analysis, a significant ($p = 0.002$) approximately 3-fold increase in the fluorescence intensity of EDEM1-specific staining in different LSG sections from several SS-patients (Fig. 3L) was detected. Also EDEM1-specific fluorescence labeling due to stroma infiltration by inflammatory cells was detected; however, this did not contribute significantly to the increase in fluorescence observed in epithelial cells of SS-patients ($p < 0.0001$) (Fig. 3M). In SS-patients, the EDEM1 staining signal in the perinuclear region was due to ER localization, as evidence by ~82% (Manders test) colocalization with PDI, an ER resident protein (Supplementary Fig. 3).

An increase in ERAD is generally ascribed to an increase in the expression and/or stability of proteins that are part of the ERAD machinery [45,46]. Here, we evaluated transcript levels of molecules involved in ERAD (see Fig. 4A) and observed a significant increase in the transcript levels of DERLIN1 ($p = 0.004$), HERP ($p = 0.005$), SEL1L ($p < 0.0001$), gp78 ($p = 0.009$), UBE2J1 ($p = 0.022$), UBE2G2 ($p = 0.001$) and p97 ($p = 0.008$) in LSG samples of SS-patients (Fig. 4B). No statistically significant differences in the mRNA levels of EDEM3 and OS-9 (Fig. 4B) were detected between the two experimental groups. In short, 7 out of 9 evaluated genes showed a significant increase in their mRNA levels in SS-patients, which is indicative of an increase in ERAD activity.

The participation of pro-inflammatory cytokines in ERAD activation was also evaluated in the 3D-acini. For DERLIN1, EDEM1 and SEL1, a significant increase in mRNA levels was detected after incubation with 1 ng/mL TNF-α or IFN-γ for short (0.5, 3, 6) and prolonged periods of time (24 h) (Fig. 4C). Similarly, protein levels of SEL1L and EDEM1 also increased significantly following treatment with either 1 ng/mL TNF-α or IFN-γ for 0.5, 3 or 6 h (Fig. 4D and E). After 24 h of stimulation with 1 (IFN-γ) and 10 ng/mL (TNF-α and IFN-γ) a significant increase in SEL1L and EDEM1 protein levels were observed (Fig. 4F and G). These results corroborate the conclusion that these pro-inflammatory cytokines increase the ERAD activity.

3.3. Role of pro-inflammatory cytokines on the expression of pro- and anti-apoptotic markers and cell survival in SG

The E3 ubiquitin ligases represent central components of the ERAD machinery that establish a functional connection between

Fig. 4. ERAD expression in LSG from controls and SS-patients and 3D-acini following stimulation with pro-inflammatory cytokines. **A**, Model depicting ERAD mechanism for processing of glycosylated and non-glycosylated substrates, as well as the proteins involved and their distribution in the ER membrane. **B**, Relative transcript levels of EDEM3, OS-9, DERLIN1, HERP, SEL1L, gp78, UBE2J1, UBE2G2 and p97 in samples of LSG from controls ($n = 7$) and SS-patients ($n = 9$). **C**, Relative transcript levels of DERLIN, SEL1L and EDEM1 in 3D-acini stimulated with or without 1 ng/mL TNF-α or IFN-γ for 0.5, 3, 6 and 24 h. **D**, Representative Western blot of SEL1L and EDEM1 in 3D-acini stimulated with 1 ng/mL TNF-α and IFN-γ for 0.5, 3 and 6 h. **E**, Protein levels of SEL1L and EDEM1 relative to β-actin in samples shown in D. **F**, Representative Western blot of SEL1L and EDEM1 in 3D-acini stimulated with 1 and 10 ng/mL TNF-α and IFN-γ for 24 h. **G**, Protein levels of SEL1L and EDEM1 relative to β-actin in samples shown in F. (*) P values lower than 0.05 were considered significant.

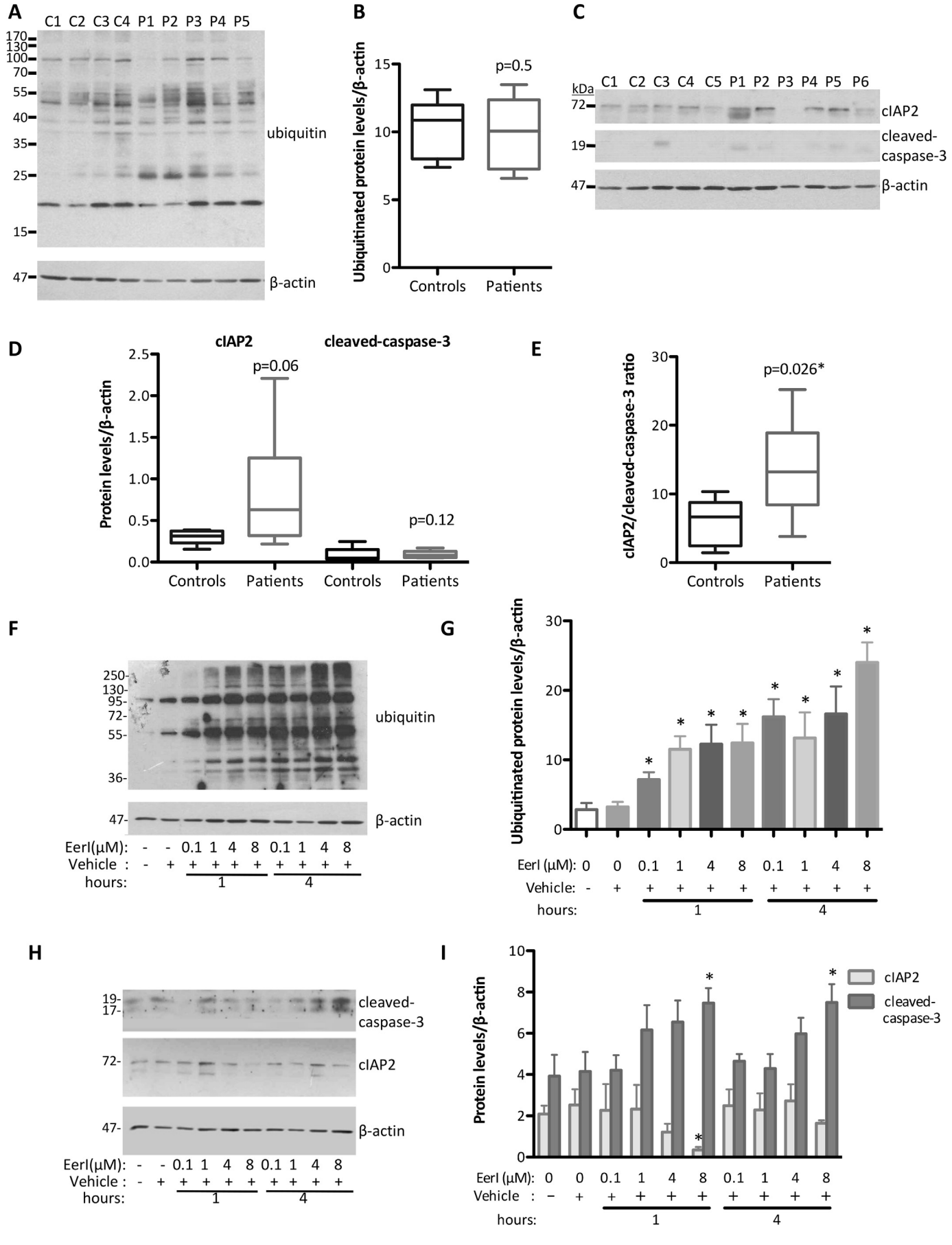
A
C1 C2 C3 C4 P1 P2 P3 P4 P5
170
130
100
70
55
40
35
25
15
ubiquitin
47
β-actin
B
Ubiquitinated protein levels/β-actin
15
10
5
0
p=0.5
Controls
Patients
C
kDa
C1 C2 C3 C4 C5 P1 P2 P3 P4 P5 P6
72
cIAP2
19
cleaved-caspase-3
47
β-actin
D
cIAP2
cleaved-caspase-3
Protein levels/β-actin
2.5
2.0
1.5
1.0
0.5
0.0
p=0.06
p=0.12
Controls
Patients
Controls
Patients
E
cIAP2/cleaved-caspase-3 ratio
30
20
10
0
p=0.026*
Controls
Patients
F
250-
130-
95-
72-
55-
36-
ubiquitin
47-
β-actin
EerI(μM): - - 0.1 1 4 8 0.1 1 4 8
Vehicle : - + + + + + + + + +
hours: 1 4
G
Ubiquitinated protein levels/β-actin
30
20
10
0
*
Eerl (μM): 0 0 0.1 1 4 8 0.1 1 4 8
Vehicle: - + + + + + + + + +
hours: 1 4
H
19-
17-
cleaved-caspase-3
72-
cIAP2
47-
β-actin
EerI(μM): - - 0.1 1 4 8 0.1 1 4 8
Vehicle : - + + + + + + + + +
hours: 1 4
I
Protein levels/β-actin
10
8
6
4
2
0
*
cIAP2
cleaved-caspase-3
Eerl (μM): 0 0 0.1 1 4 8 0.1 1 4 8
Vehicle : – + + + + + + + + +
hours: 1 4

protein quality control in the ER and the ubiquitin-proteasome system (UPS) [23]. In this context, we determined the patterns of ubiquitination of proteins in LSG of controls and SS-patients. No statistically significant differences in ubiquitination between controls and SS-patients (Fig. 5A and B) were observed.

Given the hypothesis that cytokines promote survival, we evaluated pro- and anti-apoptotic markers in LSG for both experimental groups. Apoptosis induced by ER stress depends on the activation of caspase-3 the mitochondria-dependent intrinsic pathway [47]. To calculate an apoptotic index, levels of both an apoptotic and anti-apoptotic marker of apoptosis need to be quantified. cIAP2 (BIRC3) was identified as the major anti-apoptotic gene overexpressed in a cDNA microarray study of fractions enriched in epithelial cells of LSG from SS-patients [17]. Furthermore, cIAP2 is known to be induced in response to ER stress and to be important for cell survival under such stress conditions [48]. Thus, protein levels of active caspase-3 and cIAP2 were assessed and no significant differences were detected between the two experimental groups (Fig. 5C and D); however, the cIAP2/cleaved-caspase-3 ratio increased significantly in SS-patients (Fig. 5E).

The participation of ERAD as a survival mechanism triggered by pro-inflammatory cytokines was evaluated in acini treated with EerI, a pharmacological inhibitor of p97/VCP, the ATPase involved in the translocation of ERAD substrates into the cytosol [49]. Firstly, the concentration and time required for incubation with EerI were standardized using HSG cells cultured in plates (2D), whereby the levels of protein ubiquitination, as well as of pro- and anti-apoptotic markers were determined. A significant increase in the protein levels of ubiquitinated proteins was observed after incubation with 1, 4 and 8 μM EerI for 1 and 4 h (Fig. 5F and G). A trend towards increasing active-caspase-3 protein levels after incubation with increasing concentrations of EerI was observed. This increase became significant after incubation with 8 μM EerI for either 1 or 4 h (Fig. 5H and I). Conversely, a tendency towards decreased cIAP2 protein levels was observed after incubation with increasing concentrations of Eerl. The decrease became statistically significant after incubation with 8 μM EerI for 1 h (Fig. 5H and I). No statistically significant changes in the protein levels of ubiquitinated proteins, cIAP2 and active-caspase-3 were observed in HSG cells treated with DMSO. These results show that inhibition of ERAD induces accumulation of ubiquitinated proteins, concomitant with an increase in the expression of apoptotic markers while anti-apoptotic markers decreased.

However, acini incubated with 4 or 8 μM EerI neither showed a significant increase in active-caspase-3 protein levels nor a significant decrease in cIAP2 protein levels (Fig. 6A and B), contrary to what was observed for HSG cells grown in 2D cultures on plates (Fig. 5H and I). Stimulation with pro-inflammatory cytokines (1 ng/mL TNF-α or IFN-γ) neither increased the active-caspase-3 protein levels (Fig. 6A and B). Although the band for active-caspase-3 in acini treated with TNF-α looks more intense, the β-actin band is also more pronounced resulting in no statistically significant change in the active caspase-3/β-actin ratio. It was observed that cIAP2 protein levels are significantly increased in acini treated with TNF-α, even in the presence of 4 or 8 μM EerI (Fig. 6A and B), suggesting that acini are more resistant to the stress-inducing effect of EerI compared to HSG cells in 2D.

The effect of combining pro-inflammatory cytokines and EerI was also employed to evaluate cell viability of acini (Fig. 6C and D). The results show that cell viability did not decrease in acini treated with 1 ng/mL TNF-α or IFN-γ (higher concentrations were not evaluated) (Fig. 6C and D), but did do so in acini treated with EerI for 7 h. Cytokine pre-stimulation for 12 h protected cells from death if they were subsequently co-incubated with EerI for another 7 h (Fig. 6D). However, when cytokines were extracted from the medium before adding the ERAD inhibitor, cell death was not prevented (Fig. 6C).

3.4. Correlation analysis between ATF6, ERAD and pro-inflammatory cytokines

The potential effect that pro-inflammatory cytokines may have on the expression of components of the ATF6α signaling pathway and molecules involved in ERAD was assessed using Pearson correlation analysis (Fig. 7 and Supplementary Table 3), which revealed that higher protein levels of ATF6f correlated significantly with higher protein levels EDEM1 in LSG from SS-patients. Higher levels of expression of pro-inflammatory cytokines also correlated significantly with higher protein or transcript levels of various molecules involved in ERAD (Fig. 7 and Supplementary Table 3). Higher levels of expression of pro-inflammatory cytokines correlated positively with higher transcript levels of Toll-like receptor 4 (TLR4), which was previously established for the same individuals [50] as those analyzed here. Moreover, higher TLR4 levels correlated significantly with higher levels of gp78 transcripts (Fig. 7 and Supplementary Table 3). In addition, higher levels of the ATF6f protein correlated significantly with decreased IRE1α protein levels, analyzed previously for the same individuals [15].

4. Discussion

The results of this study showed an increase in the activation of the ATF6α signaling pathway of the UPR in SG of SS-patients as also an increase in the expression of ERAD machinery components. Increased ATF6α pathway activation was specifically revealed by an increase in ATF6α transcript levels, ATF6f protein levels and ATF6α staining nuclear intensity in SG. Additionally, an increase was observed in the expression of components of the ERAD machinery, specifically in protein levels of total EDEM1 and EDEM1^{DG} and transcript levels of various molecules involved in ERAD (p97, SEL1L, gp78, UBE2J1, UBE2G2, HERP and DERLIN1). Increased expression levels of ERAD molecules and ATF6f significantly correlated with increased expression of pro-inflammatory cytokines in SG of SS-patients, as demonstrated *in vitro* in 3D-acini treated with TNF-α or IFN-γ. Moreover, cytokine stimulation increased the activation of ATF6α and ERAD without to inducing apoptosis.

The increased activation of ATF6α, together with the decreased activation of IRE1α as described previously [15], suggest a condition of chronic ER stress in SG from SS-patients. Currently, it is unclear whether the condition of chronic ER stress is a cause of cellular, molecular and functional alterations found in the SG from SS-patients or a consequence. Note that the results obtained here

Fig. 5. ERAD inhibition promotes accumulation of ubiquitinated proteins in HSG cells. A, Representative Western blot of ubiquitinated proteins in LSG extracts from control (C) and SS-patients (P). β-actin (~47 kDa) was used as a loading control. **B**, Protein levels of ubiquitinated proteins relative to β-actin in controls (n = 5) and SS-patients (n = 7) are shown as box plots. **C**, Representative Western blot of cIAP2 and cleaved-caspase-3 in LSG extracts from control and SS-patients. **D**, Protein levels of cIAP2 and cleaved-caspase-3 relative to β-actin in controls (n = 5) and SS-patients (n = 7) are shown as box plots. **E**, cIAP2/cleaved-caspase-3 protein ratio in LSG from controls and SS-patients. **F**, Representative Western blot of ubiquitinated proteins in HSG cells stimulated with EerI (0.1, 1, 4 and 8 μM) for 1 and 4 h. DMSO was used as vehicle control. **G**, Protein levels of ubiquitinated proteins relative to β-actin. **H**, Representative Western blot of cleaved-caspase-3 and cIAP2 in HSG cells stimulated with EerI (0.1, 1, 4 and 8 μM) for 1 and 4 h. **I**, Cleaved-caspase-3 and cIAP2 protein levels relative to β-actin. (*) P values lower than 0.05 were considered significant.

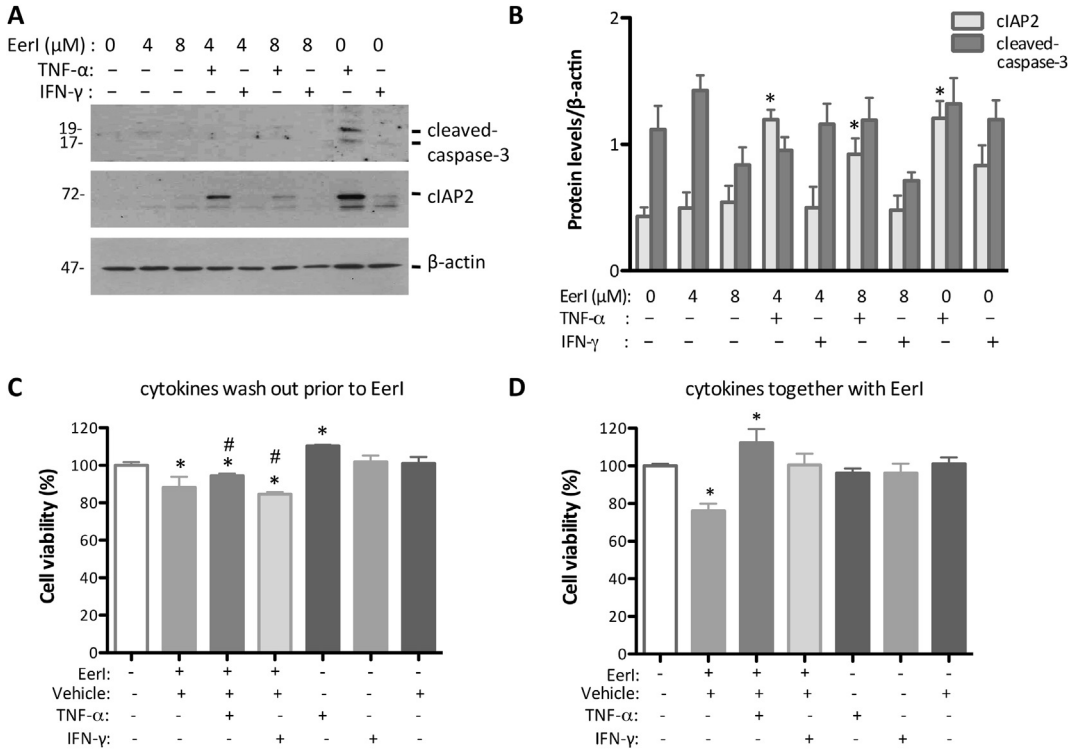

Fig. 6. Effects of pro-inflammatory cytokines on the expression of pro- and anti-apoptotic markers as well as cell viability. A, Representative Western blot of cleaved-caspase-3 and cIAP2 in 3D-acini stimulated with 4 and 8 μM EerI for 1 h and following stimulation with either 1 ng/mL TNF-α or IFN-γ in combination with 8 μM EerI for 6 h. **B**, Cleaved-caspase-3 and cIAP2 relative to β-actin. **C**, Cell viability was evaluated using the MTS/PMS assay in 3D-acini incubated with 1 ng/mL TNF-α or IFN-γ for 12 h and then with 8 μM EerI in the absence of cytokines for another 7 h. DMSO was used as vehicle control. **D**, Cell viability of 3D-acini incubated with either 1 ng/mL TNF-α or IFN-γ for 12 h and then co-incubated with 8 μM EerI for another 7 h (*) P values lower than 0.05 were considered significant.

represent a "still image" of what occurs during disease development in SS-patients. This disease is insidious and multi-symptomatic, and therefore diagnosis is often delayed [51]. As a consequence, it remains often undefined when exactly the disease begins, and consequently, how UPR relates to pathogenesis. Results from the literature show that ER stress transducers induce UPR activation in a manner dependent on duration of the inducing factors [52]. Thus, the UPR observed under chronic ER stress conditions is characterized by attenuation of the IRE1α pathway and sustained activation of ATF6α and PERK pathways [18,52–54]. Interestingly, a similar situation is observed in SG of SS-patients.

IRE1α and ATF6α pathways induce the expression of some common genes, including those involved in ERAD [19]. Given the significant decrease in XBP-1s previously reported in SG of SS-patients [15], we suggest that the increased expression of ERAD genes observed in the present study is due to a significant increase in ATF6α processing to generate ATF6f and nuclear translocation of the latter. Data from other studies indicate that SEL1L is an exclusive target of ATF6f [55], whereas that EDEM1 and HRD1 are mainly induced by XBP-1s [56,57].

For SG of control individuals activation of ATF6α pathway was also observed. Increased levels of ATF6f are indicative of elevated basal ER stress in SG controls, as has been reported in secretory cells [58]. This would appear to contradict the orthodox view of a "typical control condition", as often described for cells in culture, where low levels of ATF6f and high levels of ATF6α are observed. SG acinar cells are characterized by elevated levels of protein synthesis especially of secretory components, such as mucins, glycoproteins of high structural complexity [7]. This is likely to explain the elevated baseline stress levels observed in controls. This situation requires the activation of an adaptive UPR program without triggering cell death, as a physiologically normal response. The Western blotting results for ATF6α coincide with the almost exclusive localization of ATF6f in the nucleus observed by immunofluorescence analysis.

A significant increase in protein levels and the fluorescence intensity of EDEM1 is indicative of increased ERAD activity in SS-patients. EDEM1 is one of the most studied ERAD molecules, but its function has not yet been fully elucidated [59]. However, EDEM1 is involved in the degradation of glycosylated and non-glycosylated proteins, as well as the substrates ERAD-M and ERAD-L [43,44,59]. Also, EDEM1 overexpression increases the de-mannosylation of misfolded glycoproteins, accelerating liberation from the calnexin-calreticulin cycle and subsequent degradation by the proteasome [60]. A significant increase in $EDEM1^{DG}$ protein levels was observed in SS-patients, suggesting that ER stress is elevated SG in those patients. The higher EDEM1 protein levels in SS-patients in the absence of statistically significant differences in transcript levels may be indicative of increased translational efficiency or increased protein stability as a result of a decrease in EDEM1 turnover rate. In unstressed cells, of note, EDEM1 protein has a shorter half-life ($T_{1/2}$—55 min) than other ER resident chaperones, such as GRP78 and PDIA3 ($T_{1/2}$—120 min). Thus, the rapid turnover of EDEM1 in unstressed cells is required to maintain appropriate protein folding in the ER [46]. To the contrary, EDEM1 turnover decreases in stressed cells, resulting in elevated protein levels and ERAD activity [46]. Under physiological conditions, elevated rates of EDEM1 turnover are attributable to the formation of small vesicles derived from the ER that interact with LC3-I, termed EDEMosomes, which are degraded by lysosomal enzymes [45,46]. Thus, the accumulation of EDEM1 in the ER of SS-patients (perinuclear basal location) suggests that EDEM1 might be participating in ERAD. In addition,

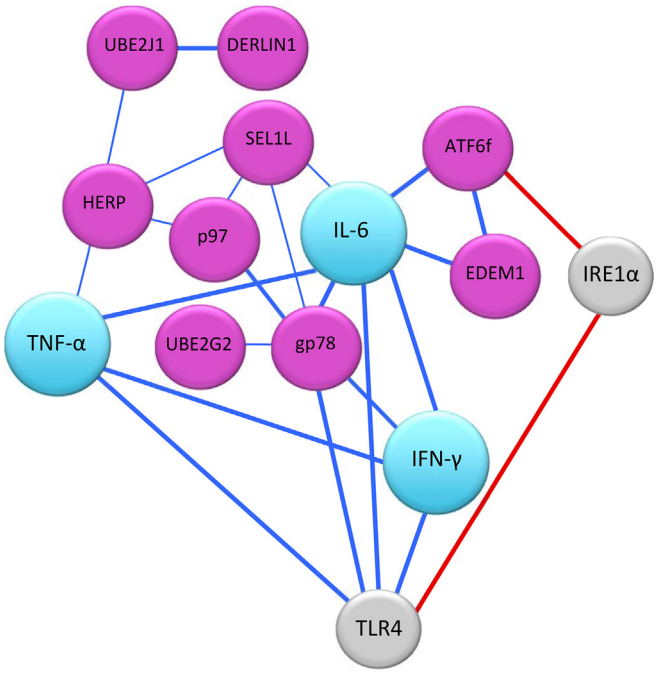

Fig. 7. Correlation network analysis considering the data set of cytokine levels, the expression of ATF6α and molecules that participate in ERAD in SG. The schematic highlights some of the most significant connections between the molecules evaluated in this study and the expression of pro-inflammatory cytokines in LSG from SS-patients and controls. A detailed list of data is provided in Supplementary Table 3. Positive and negative correlations are indicated in blue and red, respectively. Line thickness indicates correlation strength: the wider the line, the better the correlation. The mRNA levels of TLR4 and IRE1α were determined previously in the same individual group ([50] and [15], respectively). (For interpretation of the references to colour in this figure legend, the reader is referred to the web version of this article.)

EDEM1 observed in vesicle-like structures in the cytoplasm in control individuals may be indicative of low ERAD activity and an increased EDEM1 vesicle recycling (ERAD tuning) for subsequent degradation. With this in mind, increased localization of EDEM1 to the ER in SS-patients may suggest an increment in ERAD activity. High EDEM1 protein levels in SG of SS-patients were attributable to the epithelial cells. Although the inflammatory cells present in SG of SS-patients did express EDEM1, they did not contribute significantly to the increase in the fluorescence intensity.

No statistically significant differences in the levels of ubiquitinated proteins between both experimental groups were observed. However, similar levels of ubiquitinated proteins in both groups do not rule out the possibility of increased ERAD activity in SS-patients. Here, it is important to consider that the degradation of ERAD substrates is directly coupled to retro-translocation. Therefore to detect ubiquitinated ERAD substrates, inhibitors of proteasome activity are required to stabilize most ERAD substrates in the ER lumen [23]. In this scenario, differences in the degree of ubiquitination in SS patients are likely to be more difficult to detect. In addition, not all ubiquitinated proteins are ERAD substrates and cytosolic proteins also can be ubiquitinated by ERAD independent pathways.

Given that active-caspase-3 and cIAP2 can be induced by UPR under ER stress conditions they were used as cell viability markers. No statistically significant changes in the protein levels were found between both groups. However, the cIAP2/cleaved-caspase-3 ratio was significantly higher in SS-patients, indicating that apoptosis should be decreased.

The increased levels of TNF-α, IFN-γ and IL-6 in SG of SS-patients observed here corroborates data reported previously [14]. *In vitro* results showed that pro-inflammatory cytokines induce ER stress by activating the ATF6α signaling pathway. Both following acute (short times) and prolonged (24 h) induction of ER stress by stimulation with TNF-α and IFN-γ, ATF6α mRNA and protein levels, as well as ATF6f nuclear translocation were observed. The lowest concentration used (1 ng/mL) for both cytokines induced expression of ATF6α, DERLIN1 and SEL1L (the latter two being target genes of ATF6f) in a manner that was not dependent on the duration of stimulation. However, the results obtained by Western blotting and immunofluorescence analysis of 3D cultures suggest a more relevant role for IFN-γ in the activation of this pathway under acute and sustained ER stress conditions, as has been observed previously in MEFs from wild-type mice [61]. By contrast, previous results showed that IRE1α/XBP-1s pathway activation decreased after 24 h, as evidenced by decreased IRE1α sensor and transcript levels of XBP-1s [15], in agreement with the results obtained here in SG of SS-patients. Our findings are in agreement with a growing body of evidence underscoring the importance of IFN-γ in determining susceptibility to SS [17,62,63]. Importantly, increased expression of genes regulated by interferons is typically observed in many autoimmune diseases and is associated with disease development/progression [64].

Pro-inflammatory cytokines did not alter cell viability in 3D-acini and also did not affect 3D-acini pre-treated with pro-inflammatory cytokines for 12 h and then incubated with EerI in the presence of cytokines. In these experiments, increased levels of transcripts and proteins involved in ERAD were detected following 3 h–24 h of stimulation. We postulate that, once activated following cytokine stimulation, ERAD function is not affected by inhibitors of individual components in this pathway, such as p97, and cell viability is maintained. However, pre-stimulation with pro-inflammatory cytokines did not prevent cell death when cytokines were removed from the medium before blocking the ERAD machinery, indicating that the persistent presence of cytokines in the medium is necessary to maintain cell viability. Strong induction of cIAP2 was observed following incubation of 3D-acini with TNF-α, consistent with previous reports [65]. This may explain, in part why apoptosis does not increase in SG of SS-patients. In summary, our results show that pro-inflammatory cytokines under the experimental conditions employed here induced ER stress without triggering apoptosis and linked this effect to augmented cIAP2 expression.

Correlation analysis in LSG from SS-patients and controls shows that higher ATF6f protein levels correlated significantly with higher EDEM1 protein levels. Under ER stress conditions, ATF6α activation may induce an increase in the expression of molecules involved in ERAD, such as EDEM1. The overall increase in the ERAD machinery may decrease EDEM1 turnover rate, and thereby increase their protein levels. Moreover, higher levels of expression of pro-inflammatory cytokines significantly correlated with increased ATF6f and higher protein or transcript levels for various molecules involved in ERAD. Pro-inflammatory cytokines may act as agents that induce ER stress by activating the ATF6α signaling pathway and increasing transcript levels of genes involved in ERAD. In this context, it has been demonstrated that pro-inflammatory cytokines increased significantly the expression of MUC1 in HSG cells and salivary glands of SS-patients [9], which may exacerbate protein misfolding/unfolding.

In summary, the constant presence of pro-inflammatory cytokines, as well as aberrant mucin in the extracellular matrix of SG from SS-patients [39], is suggested to perpetuate the inflammatory environment, establishing a chronic ER stress condition. In this scenario, activity of the IRE1α/XBP-1s pathway appears reduced, while ATF6α and PERK (manuscript in preparation) pathways and ERAD machinery are activated. ATF6α pathway and ERAD

machinery were also activated by TNF-α and IFN-γ *in vitro* in 3D-acini preventing the death by apoptosis. IFN-γ levels were elevated in SS-patients and UPR responses triggered *in vitro* by this cytokine closely matched those observed in LSG from SS-patients, suggesting that cytokines may induce ER stress. Altogether; these findings could explain, in part, the morphological and functional alterations, as well as low levels of apoptosis found in LSG of SS-patients.

Author contributions

All authors were involved in drafting the article and revising it critically for important intellectual content, and all authors approved the final version to be published. Dr. González MJ had full access to all of the data in the study and takes responsibility for the integrity of the data and accuracy of the data analysis.

Criterion 1: a) Substantial contributions to study conception and design; and/or b) Substantial contributions to acquisition of data; and/or c) Substantial contributions to analysis and interpretation of data.

Criterion 2: Drafting the article or revising it critically for important intellectual content.

Criterion 3: Final approval of the version of the article to be published.

María-José Barrera, 1a, 1b, 1c, 2, 3.
Sergio Aguilera, 1a, 1b, 1c, 2, 3.
Isabel Castro, 1a, 1b, 1c, 2, 3.
Juan Cortés, 1b, 2, 3.
Verónica Bahamondes, 1b, 2,3.
Andrew F.G. Quest, 1c, 2, 3.
Claudio Molina, 1b, 1c, 2, 3.
Sergio González, 1b, 2, 3.
Marcela Hermoso 1c, 2, 3.
Ulises Urzúa 1c, 2, 3.
Cecilia Leyton, 1b, 2, 3.
María-Julieta González, 1a, 1b, 1c, 2, 3.

Disclosure statement

The authors have declared no conflicts of interest.

Acknowledgements

We thank all the patients who participated in this study. We gratefully acknowledge Professor Bruce Baum (NIDCR, NIH, Bethesda, MD, USA) for providing HSG cells, Dr. Patricia Burgos (Facultad de Medicina, Universidad Austral de Chile, Chile) for providing EerI, Dr. Stefana-Maria Petrescu (Institute of Biochemistry of Romanian Academy, Bucharest, Romania) for providing antibody anti-EDEM1, Dr. Claudio Hetz and Dr. René Vidal (Facultad de Medicina, Universidad de Chile) for providing PNGase F, plasmid pAAV_ATF6f and antibody anti-ATF6α, Dr. Mario Galindo (Facultad de Medicina, Universidad de Chile) for providing ELISA microplate reader and Dr. Julio Tapia (Facultad de Medicina, Universidad de Chile) for providing MTS/PMS solutions. Supported by Fondecyt-Chile [#1160015 and 1120062] (MJG, SA, CM, SG), PhD fellowship Conicyt-Chile (MJB and JC), CONICYT-FONDAP [#15130011] (AFGQ).

Appendix A. Supplementary data

Supplementary data related to this article can be found at http://dx.doi.org/10.1016/j.jaut.2016.07.006.

References

[1] H.M. Moutsopoulos, Sjogren's syndrome: autoimmune epithelitis, Clin. Immunol. Immunopathol. 72 (1994) 162–165.
[2] A.V. Goules, A.G. Tzioufas, H.M. Moutsopoulos, Classification criteria of Sjogren's syndrome, J. Autoimmun. 48–49 (2014) 42–45.
[3] S.S. Cao, K.L. Luo, L. Shi, Endoplasmic reticulum stress interacts with inflammation in human diseases, J. Cell Physiol. 231 (2016) 288–294.
[4] S.E. Bettigole, L.H. Glimcher, Endoplasmic reticulum stress in immunity, Annu. Rev. Immunol. 33 (2015) 107–138.
[5] S. Katsiougiannis, R. Tenta, F.N. Skopouli, Endoplasmic reticulum stress causes autophagy and apoptosis leading to cellular redistribution of the autoantigens Ro/Sjogren's syndrome-related antigen A (SSA) and La/SSB in salivary gland epithelial cells, Clin. Exp. Immunol. 181 (2015) 244–252.
[6] J.D. Castle, P. Arvan, R. Cameron, Protein production and secretion in exocrine cells, J. Dent. Res. (1987) 633–637, 66 Spec. No.
[7] A. Zalewska, K. Zwierz, K. Zolkowski, A. Gindzienski, Structure and biosynthesis of human salivary mucins, Acta Biochim. Pol. 47 (2000) 1067–1079.
[8] A.H. Lee, G.C. Chu, N.N. Iwakoshi, L.H. Glimcher, XBP-1 is required for biogenesis of cellular secretory machinery of exocrine glands, EMBO J. 24 (2005) 4368–4380.
[9] H.H. Sung, I. Castro, S. Gonzalez, S. Aguilera, N.I. Smorodinsky, A. Quest, et al., MUC1/SEC and MUC1/Y overexpression is associated with inflammation in Sjogren's syndrome, Oral Dis. 21 (2015) 730–738.
[10] V. Bahamondes, A. Albornoz, S. Aguilera, C. Alliende, C. Molina, I. Castro, et al., Changes in Rab3D expression and distribution in the acini of Sjogren's syndrome patients are associated with loss of cell polarity and secretory dysfunction, Arthritis Rheum. 63 (2011) 3126–3135.
[11] C. Alliende, Y.J. Kwon, M. Brito, C. Molina, S. Aguilera, P. Perez, et al., Reduced sulfation of muc5b is linked to xerostomia in patients with Sjogren syndrome, Ann. Rheum. Dis. 67 (2008) 1480–1487.
[12] T.B. Enger, M.H. Aure, J.L. Jensen, H.K. Galtung, Calcium signaling and cell volume regulation are altered in Sjogren's Syndrome, Acta Odontol. Scand. 72 (2014) 549–556.
[13] E. Goicovich, C. Molina, P. Perez, S. Aguilera, J. Fernandez, N. Olea, et al., Enhanced degradation of proteins of the basal lamina and stroma by matrix metalloproteinases from the salivary glands of Sjogren's syndrome patients: correlation with reduced structural integrity of acini and ducts, Arthritis Rheum. 48 (2003) 2573–2584.
[14] D. Sun, M.R. Emmert-Buck, P.C. Fox, Differential cytokine mRNA expression in human labial minor salivary glands in primary Sjogren's syndrome, Autoimmunity 28 (1998) 125–137.
[15] D.A.S. Sepúlveda, M.J. Barrera, V. Bahamondes, C. Castro, C. Molina, et al., SAT0380 Impaired Ire1alpha/XBP-1 pathway is associated with glandular dysfunction in Sjögren's syndrome, Ann. Rheum. Dis. 74 (2015) 796.
[16] M. Ohlsson, K. Skarstein, A.I. Bolstad, A.C. Johannessen, R. Jonsson, Fas-induced apoptosis is a rare event in Sjogren's syndrome, Lab. Invest. 81 (2001) 95–105.
[17] P. Perez, J.M. Anaya, S. Aguilera, U. Urzua, D. Munroe, C. Molina, et al., Gene expression and chromosomal location for susceptibility to Sjogren's syndrome, J. Autoimmun. 33 (2009) 99–108.
[18] J. Wu, D.T. Rutkowski, M. Dubois, J. Swathirajan, T. Saunders, J. Wang, et al., ATF6alpha optimizes long-term endoplasmic reticulum function to protect cells from chronic stress, Dev. Cell 13 (2007) 351–364.
[19] K. Yamamoto, T. Sato, T. Matsui, M. Sato, T. Okada, H. Yoshida, et al., Transcriptional induction of mammalian ER quality control proteins is mediated by single or combined action of ATF6alpha and XBP1, Dev. Cell 13 (2007) 365–376.
[20] N. Egawa, K. Yamamoto, H. Inoue, R. Hikawa, K. Nishi, K. Mori, et al., The endoplasmic reticulum stress sensor, ATF6alpha, protects against neurotoxin-induced dopaminergic neuronal death, J. Biol. Chem. 286 (2011) 7947–7957.
[21] J. Merulla, E. Fasana, T. Solda, M. Molinari, Specificity and regulation of the endoplasmic reticulum-associated degradation machinery, Traffic 14 (2013) 767–777.
[22] D. Morito, K. Nagata, Pathogenic hijacking of ER-associated degradation: is ERAD flexible? Mol. Cell 59 (2015) 335–344.
[23] J.C. Christianson, Y. Ye, Cleaning up in the endoplasmic reticulum: ubiquitin in charge, Nat. Struct. Mol. Biol. 21 (2014) 325–335.
[24] E. Jarosch, C. Taxis, C. Volkwein, J. Bordallo, D. Finley, D.H. Wolf, et al., Protein dislocation from the ER requires polyubiquitination and the AAA-ATPase Cdc48, Nat. Cell Biol. 4 (2002) 134–139.
[25] T. Amano, S. Yamasaki, N. Yagishita, K. Tsuchimochi, H. Shin, K. Kawahara, et al., Synoviolin/Hrd1, an E3 ubiquitin ligase, as a novel pathogenic factor for arthropathy, Genes Dev. 17 (2003) 2436–2449.
[26] B. Gao, K. Calhoun, D. Fang, The proinflammatory cytokines IL-1beta and TNF-alpha induce the expression of Synoviolin, an E3 ubiquitin ligase, in mouse synovial fibroblasts via the Erk1/2-ETS1 pathway, Arthritis Res. Ther. 8 (2006) R172.
[27] M. Takahata, M. Bohgaki, T. Tsukiyama, T. Kondo, M. Asaka, S. Hatakeyama, Ro52 functionally interacts with IgG1 and regulates its quality control via the ERAD system, Mol. Immunol. 45 (2008) 2045–2054.
[28] A. Espinosa, W. Zhou, M. Ek, M. Hedlund, S. Brauner, K. Popovic, et al., The Sjogren's syndrome-associated autoantigen Ro52 is an E3 ligase that regulates proliferation and cell death, J. Immunol. 176 (2006) 6277–6285.
[29] S. Scheffler, U. Kuckelkorn, K. Egerer, T. Dorner, K. Reiter, A. Soza, et al., Autoimmune reactivity against the 20S-proteasome includes immunosubunits LMP2 (beta1i), MECL1 (beta2i) and LMP7 (beta5i), Rheumatol. Oxf. 47 (2008) 622–626.

[30] E. Feist, U. Kuckelkorn, T. Dorner, H. Donitz, S. Scheffler, F. Hiepe, et al., Autoantibodies in primary Sjogren's syndrome are directed against proteasomal subunits of the alpha and beta type, Arthritis Rheum. 42 (1999) 697–702.
[31] S. Krause, U. Kuckelkorn, T. Dorner, G.R. Burmester, E. Feist, P.M. Kloetzel, Immunoproteasome subunit LMP2 expression is deregulated in Sjogren's syndrome but not in other autoimmune disorders, Ann. Rheum. Dis. 65 (2006) 1021–1027.
[32] T. Egerer, L. Martinez-Gamboa, A. Dankof, B. Stuhlmuller, T. Dorner, V. Krenn, et al., Tissue-specific up-regulation of the proteasome subunit beta5i (LMP7) in Sjogren's syndrome, Arthritis Rheum. 54 (2006) 1501–1508.
[33] S. Yamasaki, N. Yagishita, K. Tsuchimochi, K. Nishioka, T. Nakajima, Rheumatoid arthritis as a hyper-endoplasmic-reticulum-associated degradation disease, Arthritis Res. Ther. 7 (2005) 181–186.
[34] C. Vitali, S. Bombardieri, R. Jonsson, H.M. Moutsopoulos, E.L. Alexander, S.E. Carsons, et al., Classification criteria for Sjogren's syndrome: a revised version of the European criteria proposed by the American-European Consensus Group, Ann. Rheum. Dis. 61 (2002) 554–558.
[35] G.L. Schall, L.G. Anderson, R.O. Wolf, J.R. Herdt, T.M. Tarpley Jr., N.A. Cummings, et al., Xerostomia in Sjogren's syndrome. Evaluation by sequential salivary scintigraphy, JAMA 216 (1971) 2109–2116.
[36] T.E. Daniels, Labial salivary gland biopsy in Sjogren's syndrome. Assessment as a diagnostic criterion in 362 suspected cases, Arthritis Rheum. 27 (1984) 147–156.
[37] J. Debnath, S.K. Muthuswamy, J.S. Brugge, Morphogenesis and oncogenesis of MCF-10A mammary epithelial acini grown in three-dimensional basement membrane cultures, Methods 30 (2003) 256–268.
[38] Y.J. Kwon, P. Perez, S. Aguilera, C. Molina, L. Leyton, C. Alliende, et al., Involvement of specific laminins and nidogens in the active remodeling of the basal lamina of labial salivary glands from patients with Sjogren's syndrome, Arthritis Rheum. 54 (2006) 3465–3475.
[39] M.J. Barrera, M. Sanchez, S. Aguilera, C. Alliende, V. Bahamondes, C. Molina, et al., Aberrant localization of fusion receptors involved in regulated exocytosis in salivary glands of Sjogren's syndrome patients is linked to ectopic mucin secretion, J. Autoimmun. 39 (2012) 83–92.
[40] M.W. Pfaffl, G.W. Horgan, L. Dempfle, Relative expression software tool (REST) for group-wise comparison and statistical analysis of relative expression results in real-time PCR, Nucleic Acids Res. 30 (2002) e36.
[41] M.M. Bradford, A rapid and sensitive method for the quantitation of microgram quantities of protein utilizing the principle of protein-dye binding, Anal. Biochem. 72 (1976) 248–254.
[42] K. Haze, H. Yoshida, H. Yanagi, T. Yura, K. Mori, Mammalian transcription factor ATF6 is synthesized as a transmembrane protein and activated by proteolysis in response to endoplasmic reticulum stress, Mol. Biol. Cell 10 (1999) 3787–3799.
[43] M. Shenkman, B. Groisman, E. Ron, E. Avezov, L.M. Hendershot, G.Z. Lederkremer, A shared endoplasmic reticulum-associated degradation pathway involving the EDEM1 protein for glycosylated and nonglycosylated proteins, J. Biol. Chem. 288 (2013) 2167–2178.
[44] T. Tamura, J.H. Cormier, D.N. Hebert, Characterization of early EDEM1 protein maturation events and their functional implications, J. Biol. Chem. 286 (2011) 24906–24915.
[45] R. Bernasconi, C. Galli, J. Noack, S. Bianchi, C.A. de Haan, F. Reggiori, et al., Role of the SEL1L: LC3-I complex as an ERAD tuning receptor in the mammalian ER, Mol. Cell 46 (2012) 809–819.
[46] T. Cali, C. Galli, S. Olivari, M. Molinari, Segregation and rapid turnover of EDEM1 by an autophagy-like mechanism modulates standard ERAD and folding activities, Biochem. Biophys. Res. Commun. 371 (2008) 405–410.
[47] H. Shiraishi, H. Okamoto, A. Yoshimura, H. Yoshida, ER stress-induced apoptosis and caspase-12 activation occurs downstream of mitochondrial apoptosis involving Apaf-1, J. Cell Sci. 119 (2006) 3958–3966.
[48] R.B. Hamanaka, E. Bobrovnikova-Marjon, X. Ji, S.A. Liebhaber, J.A. Diehl, PERK-dependent regulation of IAP translation during ER stress, Oncogene 28 (2009) 910–920.
[49] Q. Wang, L. Li, Y. Ye, Inhibition of p97-dependent protein degradation by Eeyarestatin I, J. Biol. Chem. 283 (2008) 7445–7454.
[50] M.J. Barrera, S. Aguilera, E. Veerman, A.F. Quest, D. Diaz-Jimenez, U. Urzua, et al., Salivary mucins induce a Toll-like receptor 4-mediated pro-inflammatory response in human submandibular salivary cells: are mucins involved in Sjogren's syndrome? Rheumatol. Oxf. 54 (2015) 1518–1527.
[51] Y. Peri, N. Agmon-Levin, E. Theodor, Y. Shoenfeld, Sjogren's syndrome, the old and the new, Best. Pract. Res. Clin. Rheumatol. 26 (2012) 105–117.
[52] D.T. Rutkowski, R.J. Kaufman, That which does not kill me makes me stronger: adapting to chronic ER stress, Trends Biochem. Sci. 32 (2007) 469–476.
[53] H. Li, A.V. Korennykh, S.L. Behrman, P. Walter, Mammalian endoplasmic reticulum stress sensor IRE1 signals by dynamic clustering, Proc. Natl. Acad. Sci. U. S. A. 107 (2010) 16113–16118.
[54] Y. Hussien, D.R. Cavener, B. Popko, Genetic inactivation of PERK signaling in mouse oligodendrocytes: normal developmental myelination with increased susceptibility to inflammatory demyelination, Glia 62 (2014) 680–691.
[55] M. Kaneko, S. Yasui, Y. Niinuma, K. Arai, T. Omura, Y. Okuma, et al., A different pathway in the endoplasmic reticulum stress-induced expression of human HRD1 and SEL1 genes, FEBS Lett. 581 (2007) 5355–5360.
[56] A.H. Lee, N.N. Iwakoshi, L.H. Glimcher, XBP-1 regulates a subset of endoplasmic reticulum resident chaperone genes in the unfolded protein response, Mol. Cell Biol. 23 (2003) 7448–7459.
[57] K. Yamamoto, N. Suzuki, T. Wada, T. Okada, H. Yoshida, R.J. Kaufman, et al., Human HRD1 promoter carries a functional unfolded protein response element to which XBP1 but not ATF6 directly binds, J. Biochem. 144 (2008) 477–486.
[58] T. Teodoro, T. Odisho, E. Sidorova, A. Volchuk, Pancreatic beta-cells depend on basal expression of active ATF6alpha-p50 for cell survival even under non-stress conditions, Am. J. Physiol. Cell Physiol. 302 (2012) C992–C1003.
[59] M. Slominska-Wojewodzka, K. Sandvig, The role of lectin-carbohydrate interactions in the regulation of ER-associated protein degradation, Molecules 20 (2015) 9816–9846.
[60] S. Olivari, T. Cali, K.E. Salo, P. Paganetti, L.W. Ruddock, M. Molinari, EDEM1 regulates ER-associated degradation by accelerating de-mannosylation of folding-defective polypeptides and by inhibiting their covalent aggregation, Biochem. Biophys. Res. Commun. 349 (2006) 1278–1284.
[61] P. Gade, G. Ramachandran, U.B. Maachani, M.A. Rizzo, T. Okada, R. Prywes, et al., An IFN-gamma-stimulated ATF6-C/EBP-beta-signaling pathway critical for the expression of Death Associated Protein Kinase 1 and induction of autophagy, Proc. Natl. Acad. Sci. U. S. A. 109 (2012) 10316–10321.
[62] C.Q. Nguyen, A.B. Peck, The interferon-signature of Sjogren's syndrome: how unique biomarkers can identify underlying inflammatory and immunopathological mechanisms of specific diseases, Front. Immunol. 4 (2013) 142.
[63] J.C. Hall, L. Casciola-Rosen, A.E. Berger, E.K. Kapsogeorgou, C. Cheadle, A.G. Tzioufas, et al., Precise probes of type II interferon activity define the origin of interferon signatures in target tissues in rheumatic diseases, Proc. Natl. Acad. Sci. U. S. A. 109 (2012) 17609–17614.
[64] L. Ronnblom, M.L. Eloranta, The interferon signature in autoimmune diseases, Curr. Opin. Rheumatol. 25 (2013) 248–253.
[65] G.J. Gordon, M. Mani, L. Mukhopadhyay, L. Dong, B.Y. Yeap, D.J. Sugarbaker, et al., Inhibitor of apoptosis proteins are regulated by tumour necrosis factor-alpha in malignant pleural mesothelioma, J. Pathol. 211 (2007) 439–446.